Experiments in Fluids 36 (2004) 879–887
DOI 10.1007/s00348-003-0770-2

Experimental study of turbulent thermal diffusion in oscillating grids turbulence

J. Buchholz, A. Eidelman, T. Elperin, G. Grünefeld, N. Kleeorin, A. Krein, I. Rogachevskii

Abstract We have experimentally detected a new effect, turbulent thermal diffusion, as predicted theoretically by Elperin et al. (Phys Rev Lett (1996) 76:224–228) and associated with the turbulent transport of inertial particles. The essence of this effect is an appearance of a non-diffusive mean flux of particles in the direction of the mean heat flux. This results in formation of large-scale inhomogeneities in the spatial distribution of inertial particles that are accumulated in regions of minimum mean temperature in the surrounding fluid. The experiments were performed in oscillating grids turbulence with an imposed mean temperature gradient. We used Particle Image Velocimetry to determine the turbulent velocity field, and an Image Processing Technique based on the analysis of the intensity of the Mie scattering to determine the spatial distribution of tracer particles. Analysis of the intensity of laser light Mie scattering by tracer particles showed that the tracer particles accumulate in the vicinity of the minimum of the mean temperature. The latter finding confirms the existence of the effect of turbulent thermal diffusion.

1 Introduction

It is generally believed that turbulence promotes mixing (McComb 1990; Stock 1996). However, experiments show the formation of long-living inhomogeneities in the number density distribution of small inertial particles in turbulent fluid flows (Eaton and Fessler 1994). The origin of these inhomogeneities is not always clear, but their influence on mixing can hardly be overestimated.

The problem of how aerosol clouds form is of fundamental significance in many areas of environmental science, physics of the atmosphere and meteorology. It is well-known that turbulence results in the decay of inhomogeneities of aerosol concentration due to turbulent diffusion, whereas the opposite effect, the preferential concentration of aerosols in atmospheric turbulent fluid flow, is a subject of much discussion.

In our previous studies (Elperin et al. 1996a, 1996b, 1997, 1998a, 1998b, 2000a, 2000b, 2000c, 2001, 2002), we predicted a number of new effects associated with turbulent transport of particles. These effects, namely turbulent thermal diffusion and clustering instability, are related to the interaction between small inertial particles and turbulent flows, and result in the formation of large-scale and small-scale inhomogeneities in particle spatial distribution.

The main goal of this paper is to describe the experimental detection of a new physical phenomenon of turbulent thermal diffusion, which was predicted theoretically by Elperin et al. (1996a, 1997). The phenomena of molecular thermal diffusion in gases (Enskog 1911; Chapman 1917; Chapman and Dootson 1917) and thermophoresis of particles (Tyndall 1870) were found long ago. The equation for the number density n of particles, taking into account these effects, reads $\frac{\partial n}{\partial t} = -\nabla \cdot \mathbf{J}_{\mathrm{M}}$, where the flux of particles J_{M} is given by $\mathbf{J}_{\mathrm{M}} = -D\left(\nabla n + \frac{k_{\mathrm{t}} \nabla T}{T}\right)$. The first term in the formula for the flux of particles describes molecular diffusion, while the second term accounts for the flux of particles caused by the fluid temperature gradient ∇T (molecular thermal diffusion or thermophoresis). Here $D$is the coefficient of molecular diffusion, $k_{\mathrm{t}} \propto n$ is the thermal diffusion ratio, and D_{M}=Dk_{t} is the coefficient of molecular thermal diffusion. In turbulent fluid flow with large Reynolds and Peclet numbers, the nature of diffusion drastically changes; for instance, turbulence results in a sharp increase of the effective diffusion coefficient (Taylor 1921).

It was found by Elperin et al. (1996a, 1997, 1998a, 2000b, 2001) that in a low Mach number turbulent fluid flow with a non-zero mean temperature gradient an additional mean flux of particles appears in the direction opposite to the mean temperature gradient (the phenomenon of turbulent thermal diffusion). For large Reynolds and Peclet numbers, the turbulent thermal diffusion is much stronger than the molecular thermal diffusion. The evolution of the number density $n(t, \mathbf{r})$ of small particles in a turbulent flow is determined by the following equation:

Received: 14 November 2002 / Accepted: 6 December 2003
Published online: 19 March 2004

J. Buchholz, G. Grünefeld
Faculty of Mechanical Engineering, RWTH Aachen University, Aachen, Germany

A. Eidelman, T. Elperin (✉), N. Kleeorin, A. Krein, I. Rogachevskii
The Pearlstone Center for Aeronautical Engineering Studies, Department of Mechanical Engineering, The Ben-Gurion University of the Negev, POB 653, 84105 Beer-Sheva, Israel
E-mail: elperin@menix.bgu.ac.il

We are indebted to F. Busse, H.J.S. Fernando, J. Katz, E. Kit, V. L'vov, J. Mann, S. Ott and A. Tsinober for illuminating discussions. This work was partially supported by the German-Israeli Project Cooperation (DIP), administered by the Federal Ministry for Education and Research (BMBF) and by the Israel Science Foundation (governed by the Israeli Academy of Science).

$$\frac{\partial n}{\partial t} + \nabla \cdot \left(n\,\mathbf{v}_\mathrm{p}\right) = -\nabla \cdot \mathbf{J}_\mathrm{M}, \tag{1}$$

where $\mathbf{v}_\mathrm{p}$ is the velocity field acquired by the particles in a turbulent fluid velocity field. Averaging Eq. 1 over the turbulent velocity field, we arrive at the equation for the mean number density of particles $\bar{N} \equiv \langle n \rangle$:

$$\frac{\partial \bar{N}}{\partial t} + \nabla \cdot \left(\bar{N}\,\bar{\mathbf{V}}_\mathrm{p}\right) = -\nabla \cdot (\bar{\mathbf{J}}_\mathrm{T} + \bar{\mathbf{J}}_\mathrm{M}), \tag{2}$$

$$\bar{\mathbf{J}}_\mathrm{T} = \bar{N}\,\mathbf{V}_\mathrm{eff} - \hat{D}\nabla\bar{N}, \tag{3}$$

where $\hat{D} \equiv D_{ij} = \langle \tau u_i u_j \rangle$is the turbulent diffusion tensor, τ is the momentum relaxation time of the turbulent velocity field, $\mathbf{v}_\mathrm{p} = \bar{\mathbf{V}}_\mathrm{p} + \mathbf{u}$, $\bar{\mathbf{V}}_\mathrm{p} = \langle \mathbf{v}_\mathrm{p} \rangle$is the mean particle velocity,

$$\mathbf{V}_\mathrm{eff} = -\langle \tau \mathbf{u} (\nabla \cdot \mathbf{u}) \rangle \tag{4}$$

is the effective velocity, $\bar{\mathbf{J}}_\mathrm{M} = -D\left(\nabla\bar{N} + \frac{k_\mathrm{t}\nabla\bar{T}}{\bar{T}}\right)$ is the mean molecular flux of particles, and $\bar{T} = \langle T \rangle$ is the mean fluid temperature. The effective mean velocity of particles implies an additional mean non-diffusive flux of particles, which can result in the formation of large-scale inhomogeneities in particle spatial distribution. Equations 2 and 3 were rigorously derived by different methods (see Elperin et al. 1996a, 1997, 1998a, 2000b, 2001; Pandya and Mashayek 2002).

The turbulent flux of particles can also be estimated using simple qualitative arguments. Indeed, let us average Eq. 1 over the turbulent velocity field and subtract the averaged equation obtained from Eq. 1. This yields the equation for the turbulent component q of particle number density:

$$\frac{\partial q}{\partial t} - D\Delta q + \nabla \cdot \mathbf{Q} = -\nabla \cdot (\bar{N}\mathbf{u}), \tag{5}$$

where $n = \bar{N} + q$ and $\mathbf{Q} = \mathbf{u}q - \langle \mathbf{u}q \rangle$. This equation is written in a frame moving with the local mean velocity $\bar{\mathbf{V}}_\mathrm{p}$. At large Reynolds numbers in the inertial range of turbulence, the LHS of this equation can be estimated as q/τ. Therefore, the fluctuations in particle number density q are of the order of $q \sim -\tau\bar{N}(\nabla \cdot \mathbf{u}) - \tau(\mathbf{u} \cdot \nabla)\bar{N}$. Multiplying the latter equation by $\mathbf{u}$ and averaging it over the turbulent velocity field, we obtain Eq. 3 for the turbulent flux of particles, $\bar{\mathbf{J}}_\mathrm{T} \equiv \langle \mathbf{u}q \rangle$.

For non-inertial particles advected by a low Mach number turbulent fluid flow, the particle velocity $\mathbf{v}_\mathrm{p}$ coincides with the fluid velocity $\mathbf{v}$, and

$$\nabla \cdot \mathbf{v} \approx -\frac{(\mathbf{v} \cdot \nabla)\rho}{\rho} \approx \frac{(\mathbf{v} \cdot \nabla)T}{T}. \tag{6}$$

Therefore, the effective velocity is given by

$$\mathbf{V}_\mathrm{eff} = -D_\mathrm{T}\frac{\nabla\bar{T}}{\bar{T}}, \tag{7}$$

where $D_\mathrm{T} = \left(\frac{\tau}{3}\right)\langle \mathbf{u}^2 \rangle$is the turbulent diffusion coefficient and ρ is the density of the fluid. Here we used the equation of state of the ideal gas and neglected small gradients of the mean fluid pressure.

For inertial particles, the velocity $\mathbf{v}_\mathrm{p}$ depends on the velocity of the surrounding fluid $\mathbf{v}$, and it can be determined from the equation of motion for a particle. Solution of the equation of motion for small particles with $\rho_\mathrm{p} \gg \rho$ yields: $\mathbf{v}_\mathrm{p} = \mathbf{v} - \tau_\mathrm{p}\frac{d\mathbf{v}}{dt} + \mathrm{O}\left(\tau_\mathrm{p}^2\right)$(see Maxey 1987), where τ_p is the Stokes time, ρ_p is the material density of particles. Then

$$\nabla \cdot \mathbf{v}_\mathrm{p} = \nabla \cdot \mathbf{v} + \tau_\mathrm{p}\frac{\Delta P}{\rho} + \mathrm{O}\left(\tau_\mathrm{p}^2\right) \tag{8}$$

(Elperin et al. 1996a, 1997), and the effective velocity is $\mathbf{V}_{eff} = -D_T(1+\kappa)\frac{\nabla\bar{T}}{\bar{T}}$, where the coefficient κ depends on the particle inertia (m_p/m_μ), the parameters of turbulence (Reynolds number) and the mean fluid temperature (Elperin et al. 1996a, 1997, 1998a, 2000b, 2001), where m_p is the particle mass and m_μ is the mass of molecules of the surrounding fluid.

The turbulent flux of particles can be rewritten as

$$\bar{\mathbf{J}}_\mathrm{T} = -D_\mathrm{T}\left[k_\mathrm{T}\frac{(\nabla\bar{T})}{\bar{T}} + \nabla\bar{N}\right], \tag{9}$$

where $k_\mathrm{T} = (1+\kappa)\bar{N}$ can be interpreted as the turbulent thermal diffusion ratio, and $D_\mathrm{T}k_\mathrm{T}$ is the coefficient of turbulent thermal diffusion. The phenomenon of turbulent thermal diffusion results in large-scale pattern formation whereby the initial spatial distribution of particles in a turbulent fluid flow evolves into a large-scale inhomogeneous distribution; in other words the particles are accumulated in the vicinity of the minimum of the mean temperature of the surrounding fluid (Elperin et al. 1996a, 1997, 1998a, 2000b, 2001).

The mechanism of this effect for $\rho_\mathrm{p} \gg \rho$ is as follows. The inertia causes particles inside the turbulent eddies to drift out to the boundary regions between eddies (in other words, regions with low vorticity or high strain rate and maximum of fluid pressure). Therefore, particles are accumulated in regions with maximum pressure of the turbulent fluid. Indeed, consider the pure inertia effect (in other words let $\nabla\cdot\mathbf{v}=0$). The inertia effect results in $\nabla \cdot \mathbf{v}_p \propto \tau_p\Delta\mathbf{P} \neq 0$. On the other hand, Eq. 1 for large Peclet numbers yields $\nabla \cdot \mathbf{v}_\mathrm{p} \propto -\frac{dn}{dt}$. This implies that $\frac{dn}{dt} \propto -\tau_\mathrm{p}\Delta P$; in other words, in regions with maximum pressure of the turbulent fluid (where $\Delta P<0$) there is an accumulation of inertial particles ($dn/dt>0$). Similarly, there is an outflow of particles from regions with minimum pressure of fluid. In homogeneous and isotropic turbulence without large-scale external gradients of temperature, a drift from regions with increased or decreased concentrations of particles by a turbulent flow of fluid is equiprobable in all directions, and pressure and temperature of the surrounding fluid are not correlated with turbulent velocity field. This means that only turbulent diffusion of particles exists.

The situation drastically changes in a turbulent fluid flow with a mean temperature gradient. In this case the mean heat flux $\langle \mathbf{u}\theta \rangle$ is not zero – fluctuations of fluid temperature θ and velocity of the fluid are correlated. Fluctuations of temperature cause fluctuations of pressure of the fluid, and the pressure fluctuations result in fluc-

tuations of the number density of particles. Increase of the pressure of the surrounding fluid is accompanied by accumulation of the particles. Therefore, the direction of the mean flux of the particles coincides with that of the heat flux, $\langle \mathbf{v}_p n \rangle \propto \langle \mathbf{u}\theta \rangle \propto -\nabla \bar{T}$, so the mean flux of particles is directed to the minimum of the mean temperature, and the particles are accumulated in this region.

Indeed, in a fluid flow with an imposed mean temperature gradient, pressure and velocity fluctuations are correlated, and regions with a higher level of pressure fluctuations have higher temperature and velocity fluctuations. Assume that the mean temperature at the point r_2 is larger than that at the point r_1, and let us direct the x-axis in the direction of the heat flux. Consider two small control volumes a and b located between these two points, and let the local turbulent velocity at the control volume a be directed at some instant, as is the heat flux (to the point r_1). Let the local turbulent velocity at the control volume b be directed at this instant in the opposite direction to the heat flux (to the point r_2). Therefore, the fluctuations of the temperature and pressure at the control volume a are positive, and at the control volume b they are negative. The fluctuations of the particle number density are positive in the control volume a(because particles are locally accumulated in the vicinity of the maximum of pressure fluctuations), and they are negative at the control volume b (because there is an outflow of particles from regions with a low pressure). The mean flux of particles is positive in the control volume a (it is directed to the point r_1), and it is also positive at the control volume b (because fluctuations of both velocity and number density of particles are negative at the control volume b). Therefore, the mean flux of particles is directed, as is the heat flux, towards the point r_1.

The effect of turbulent thermal diffusion is important in atmospheric phenomena (for instance, atmospheric aerosols, cloud formation and smog formation), and industrial turbulent flows (such as internal combustion engines). In particular, this effect results in the formation of large-scale inhomogeneities in the spatial distribution of aerosol particles. Localization of these inhomogeneities is correlated with temperature inversion regions in atmospheric turbulence.

The main goal of this study is to experimentally investigate the effect of turbulent thermal diffusion. An oscillating grids turbulence generator was constructed to study this effect (Eidelman et al. 2002). The observation time in the oscillating grids turbulence generator is almost unlimited due to the small mean velocity of the flow. A stable mean temperature gradient was formed in the core of a turbulent flow. Particle image velocimetry (PIV) was used to determine a turbulent velocity field, and an image processing technique based on Mie scattering was employed to determine the spatial distribution of particles.

2
Experimental set-up

The experiments were carried out in a specially constructed set-up where turbulence is generated by oscillating grids in the air. The test section was constructed as a rectangular chamber of dimensions 29×29×58 cm.

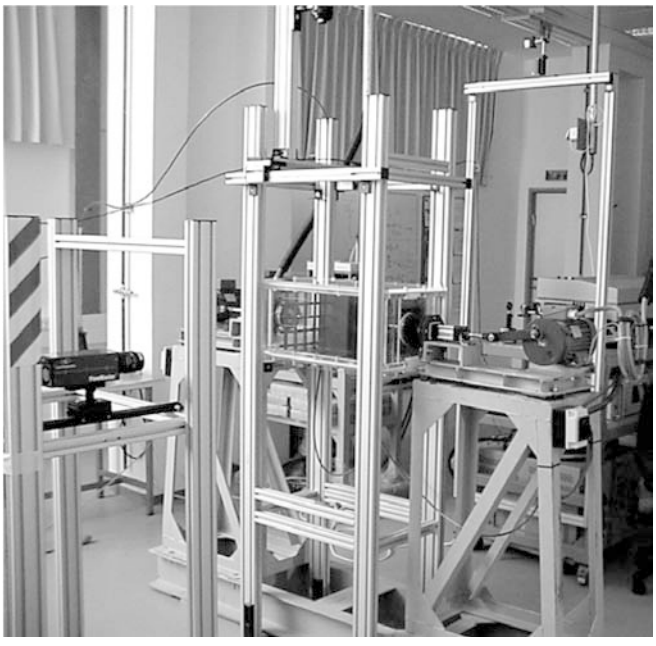

Fig. 1. The experimental set-up

A photograph of the experimental set-up is shown in Fig. 1, and other photographs can be found on the Web (http://www.bgu.ac.il/me/laboratories/tmf/equipment.html). The test section is shown in Fig. 2. Pairs of vertically-oriented grids, with bars arranged in a square array are attached to the right and left horizontal rods. Both grids are driven independently with speed-controlled motors. The grids are positioned at a distance of two grid meshes from the chamber walls parallel to them. This two grids system is capable of oscillating at a controllable frequency up to 20 Hz. The grid stroke was adjusted in a range up to 10 cm. Hereafter we use the following system of coordinates: Z is the vertical axis, the Y-axis is perpendicular to the grids, and the XZ-plane is parallel to the grids plane.

In previous experimental studies (Thompson and Turner 1975; Hopfinger and Toly 1976; Kit et al. 1997) of turbulence generated by one oscillating grid in a water tank, some useful relations were found. In particular, the

Fig. 2. The test section of the oscillating grids turbulence

dependencies of turbulent velocity u and the turbulence integral scale L on the distance from the grid mid-position Y, the mesh size M, the frequency f and the stroke S of the grid oscillations were obtained. The expression for the turbulent velocity reads:

$$u = c_u c_s^{\frac{3}{2}} \frac{fM^2}{Y}, \quad (10)$$

where the coefficients $c_u \approx 0.25$ and $c_s = S/M$. The turbulence integral scale is proportional to the distance from a grid, $L = c_l Y$, where the coefficient c_l varied over the range 0.086–0.125 in different experiments. Recent studies (Kit et al. 1997) of oscillating grid turbulence confirmed these relations. Studies of the oscillating grid turbulence showed that it has the local properties of isotropic turbulence (De Silva and Fernando 1994). A region with approximately homogeneous and isotropic turbulence is formed between two oscillating grids (Srdic et al. 1996). It was found by Shy et al. (1997) that the length of this region is linearly proportional to the distance between the grids.

Our estimates of the turbulence integral scale dependence versus the distance Y, based on data from Hopfinger and Toly (1976) for a range of c_s values from 0.2–0.9 yields $L = c_0 c_s^{\frac{3}{2}} Y$ with $c_0 = 0.25$. Using the above relations for the characteristic turbulent velocity and the turbulence integral scale, we estimated the Reynolds number:

$$\mathrm{Re} \equiv \frac{uL}{v} = c_u c_0 c_s^2 \frac{fM^2}{v}, \quad (11)$$

where v is the kinematic viscosity. Equation 11 shows that the Reynolds number is independent of the distance from the grid Y. These relations for turbulence characteristics were used in the design of our experimental set-up.

A mean temperature gradient in the turbulent flow was formed with two aluminum heat exchangers attached to the bottom (cold) and top (hot) walls of the test section (see Fig. 2). In order to improve heat transfer in the boundary layers at the walls, we used a heat exchanger with rectangular fins (3×3×15 mm) which allowed us to support a mean temperature gradient in the core of the flow up to 200 K/m at a mean temperature of about 300 K.

3 Instrumentation

The turbulent velocity field was measured using a Particle Image Velocimetry (PIV) system (see Raffel et al. 1998). We used a digital PIV system with LaVision Flow Master III. A double-pulsed light sheet is provided by a Nd-YAG laser source (Continuum Surelite 2×170 mJ). The light sheet optics comprised spherical and cylindrical Galilei telescopes with tuneable divergence and adjustable focus length. A progressive-scan 12 bit digital CCD camera (pixels with a size 6.7 μm × 6.7 μm each) was used, with a dual-frame-technique for cross-correlation processing of captured images. A programmable Timing Unit (PC interface card) generates sequences of pulses to control the laser, the camera and data acquisition. The software package DaVis 6 was applied to control all hardware components and for 32 bit image acquisition and visualization. DaVis 6 comprises PIV software for calculating the flow fields using a cross-correlation analysis. Velocity maps and their characteristics, such as statistics and PDF, were analyzed with this package and additional software. An incense smoke with sub-micron particles (with $\rho_p/\rho \sim 10^3$) as the tracer was used for PIV measurements. Smoke was produced by high temperature sublimation of solid incense particles. Analysis of smoke particles using a microscope (Nikon, Epiphot with an amplification of 560) and a PM-300 portable laser particulate analyzer showed that these particles have an approximately spherical shape with mean diameter 0.7 μm.

We determined the mean and r.m.s. velocities, two-point correlation functions, and an integral scale of turbulence from the measured velocity fields. A series of 100 pairs of images acquired with a frequency of 4 Hz was stored for calculating velocity maps and for ensemble and spatial averaging of turbulence characteristics. Velocity maps with 32×32 vectors were determined in two planes: parallel to the grid (the one grid experiments), and perpendicular to the grids (the two grids experiments).

The center of the measurement region coincides with the center of the chamber. We measured velocity for flow areas from 60×60 mm^2 up to 212×212 mm^2 with a spatial resolution of 1024×1024 pixels. This corresponds to spatial resolutions 58–207 μm/pixel. These measurement regions were analyzed with interrogation windows of 32×32 and 16×16 pixels. In every interrogation window a velocity vector was determined. This allowed us to construct the velocity map comprising 32×32 or 64×64 vectors.

The velocity maps can be considered as independent, since the maximum correlation time of turbulence is $L/u \leq 0.15$ s, while the time interval between pairs of images is 0.25 s. The mean and r.m.s. velocities for each point of a velocity map (1024 points) were calculated by averaging over 100 independent maps, and then they were averaged over 1024 points. The two-point correlation functions of the velocity field were calculated for every point of the central part of the velocity map (with 16×16 vectors) by averaging over 100 independent velocity maps, and then they were averaged over 256 points. An integral scale L of turbulence was determined from the two-point correlation functions of the velocity field. These measurements were repeated for different distances from the grid, various temperature gradients, Reynolds numbers and particle mass loadings.

The effect of Mie light scattering by particles was used to determine the particle spatial distribution in the flow (Becker et al. 1967). The advantages of using this method with a CCD camera for registration and laser sheet lighting were demonstrated by Guibert et al. (2001). The intensity distribution of the scattered light was determined in our experiments with the developed software.

The central 20×20 cm region of the chamber was probed. The mean intensity of the scattered light was determined in 32×16 interrogation windows with 32×64 pixels. The vertical distribution of the intensity of the scattered light was determined in 16 vertical strips composed of 32 interrogation windows. The light radiation energy flux scattered by small particles is $E_s \propto E\Psi\left(\frac{\pi d_p}{\lambda}; a; n\right)$, where $E \propto \frac{\pi d_p^2}{4}$ is the energy flux incident at the particle, d_p is the

particle diameter, λ is the wavelength, a is the index of refraction and Ψ is the scattering function. For wavelengths λ which are larger than the particle perimeter ($\lambda > \pi d_p$), the function Ψ is given by Rayleigh's law: $\Psi \propto d_p^4$. If the wavelength is small, the function Ψ tends to be independent of d_p and λ. In the general case, the function Ψ is given by Mie's equations (see, for example, Bohren and Huffman 1983). The scattered light energy flux incident on the CCD camera probe (producing proportional charge in every CCD pixel) is proportional to the particle number density n, in other words, $E_s \propto En\left(\frac{\pi d_p^2}{4}\right)$. The probability density function for the particle size (measured with the PM300 particulate analyzer) is independent of the location in the flow. Indeed, since the number density of particles is small, so that they are about 1 mm apart, it can be safely assumed that a change in particle number density n does not affect their size distribution. Therefore, the ratio of the scattered radiation fluxes at two points and at the image measured with the CCD camera is equal to the ratio of the particle mean number densities at these two locations. Mie scattering hardly changes due to temperature effects because it depends on the electric permittivity of particles, the particle size and the laser light wavelength. The temperature effect on these characteristics is negligibly small.

4 Results

Turbulent flow parameters in the oscillating grids turbulence generator are as follows: the Taylor scale is about 5 mm and the Kolmogorov length scale η is about 400 μm. The spatial resolution of the conducted PIV measurements was about 5 η, and this magnitude of spatial resolution is sufficient for characterization of the second moments of the turbulent velocity field (Sandham 2001). The measurements demonstrate a wide range of scales of turbulent motions. Remarkably, a flow with a wide range of spatial scales has already formed by comparatively low frequencies of grids oscillations. We found a weak mean flow in the form of two large toroidal structures parallel and adjacent to the grids. The interaction of these structures results in symmetric mean flow that is sensitive to the parameters of grids adjustment. We studied the parameters that affect the mean flow such as the grids distance to the walls of the chamber and partitions, the angles of the grids planes with the axes of their oscillation, and so on. This study allowed us to expand the central region with homogeneous turbulence. The measured r.m.s. velocity was five times higher than the mean velocity in the core of the flow.

We determined the dependence of the turbulence integral scale on the distance Y from the grid. These experiments were conducted with one oscillating grid. For instance, the dependence of a turbulent integral scale versus the distance Y from the grid oscillating at a frequency f=10.4 Hz is shown in Fig. 3. The turbulence integral scale grows up to the distance Y/M=5.6, with the coefficient c_l=0.148 (up to the maximum integral scale L=0.72 M).

The dependence of the r.m.s. velocity on the frequency of the grid oscillations measured at the distance Y/M=5.6 from the grid is shown in Fig. 4. It is described well by Eq. 10 with the coefficient c_u=0.255, in agreement with Hopfinger and Toly (1976). The results of our experiments showed that the r.m.s. velocity components u_x and u_z (in the plane parallel to the grid) are fairly isotropic. R.m.s velocity components measured at grids oscillation frequency f=10.5 Hz are shown in Fig. 5 for a wide range of distances Y from the grid. This dependence is slightly nonlinear over the measured range of distances Y from the grid, probably because the range of Y is two times wider than that in previous studies. Results shown in Figs. 3 and 5 demonstrate that the integral scale of turbulence is linearly proportional to the distance from the grid, while the

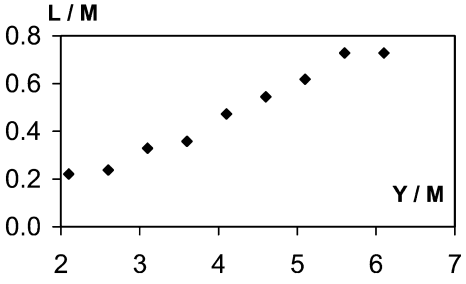

Fig. 3. Integral scale of turbulence versus distance Y from the grid at frequency of grids oscillations f=10.5 Hz

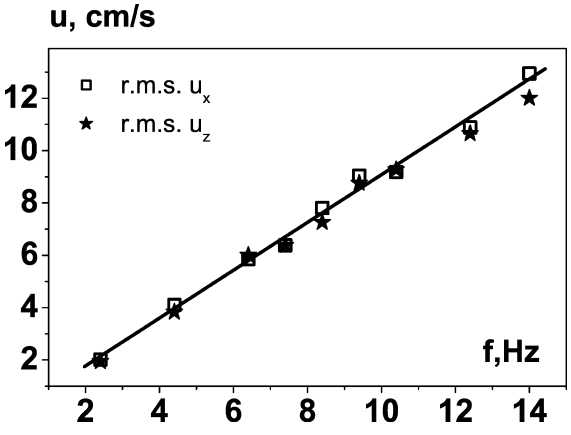

Fig. 4. Dependence of r.m.s. velocity components u_x and u_z on the frequency f of grids oscillations

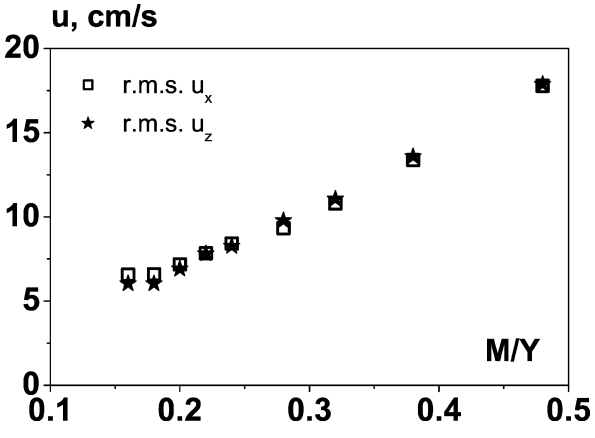

Fig. 5. R.m.s. velocity components u_x and u_z versus the inverse distance M/Y from the grid

r.m.s. velocity is inversely proportional to the distance from the grid in the central part of the flow. Therefore, the Reynolds number (see Eq. 11) and the turbulent diffusion coefficient $D_z^T = u_z L_z$ for particles are almost independent of the distances from the grid.

Temperature measurements were conducted in the oscillating grids turbulence generator. The temperature difference between the heat exchangers varied over the range 25–50 K. The mean temperature vertical profile in the chamber is shown in Fig. 6. The mean temperature gradient in the core of the flow attained a magnitude of 118 K/m, that was sufficient for investigation of the phenomenon of turbulent thermal diffusion.

Measurements performed using different concentrations of the incense smoke in the flow showed that the distribution of the scattered light intensity (normalized by averaging over the vertical coordinate light intensity) is independent of the mean particle number density in the isothermal flow. Measured dependencies of the normalized light intensity ratios $E_r^* = \frac{E_{r,k}}{E_{r,m}}$ versus the vertical coordinate Z are shown in Fig. 7. Here the subscripts k and m denote results obtained in different experiments with the isothermal flow. The differences between the curves in Fig. 7 (less than 0.8%) are caused by the uncertainties in optics adjustment, errors in measuring a CCD image background value, and so on. These experimental uncertainties are considerably smaller than the observed effect of a 10–15% change in the normalized intensity of the scattered light in the test section in the presence of the imposed mean temperature gradient. A very weak dependence of the normalized light intensities on the mean particle number density (shown in Fig. 7) demonstrates that the particles-air suspension can be considered as an optically thin medium for the studied range of tracer concentrations. The latter allows us to conclude that the intensity of the scattered light is proportional to the particle number density.

In order to characterize the spatial distribution of particle number density $\bar{N}$ in the non-isothermal flow, the

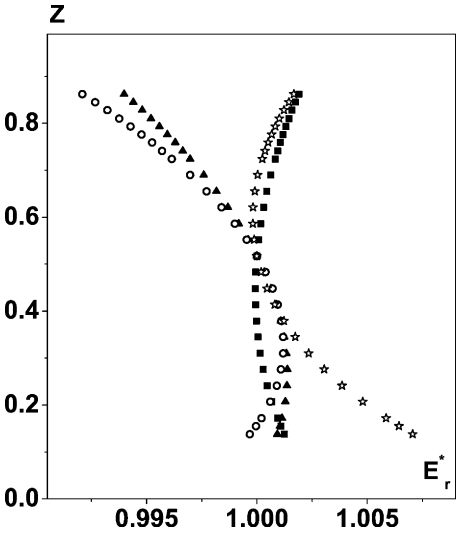

Fig. 7. Ratio $E_r^* = \frac{E_{r,k}}{E_{r,m}}$ of the normalized scattered light intensities versus the vertical coordinate Z, obtained from different investigations of the isothermal flow

distribution of the scattered light energy flux E_r measured in the isothermal case was used for the normalization of the scattered light energy flux E_r^T obtained in a non-isothermal flow under the same optical conditions; in other words, $\bar{N} \propto \frac{E_r^T}{E_r}$. Here the radiation fluxes E_r^T and E_r in each experiment are normalized by the corresponding radiation fluxes averaged over the vertical coordinate. The dependencies of E_r^T and E_r, approximated by a smoothing function, were used for plotting the dependence of $N_r \equiv \frac{\bar{N}}{\bar{N}_0}$ versus $T_r \equiv \frac{(\bar{T}-\bar{T}_0)}{\bar{T}_0}$, where $\bar{T}_0$ is the reference temperature and $\bar{N}_0 = \bar{N}(\bar{T} = \bar{T}_0)$. The dependence of the normalized particle number density N_r on the normalized temperature difference T_r is shown in Fig. 8. The results shown in Fig. 8 were obtained by averaging over the data obtained in eight experiments. The vertical distribution of the intensity of the scattered light was determined in 16 vertical strips composed of 32 interrogation windows.

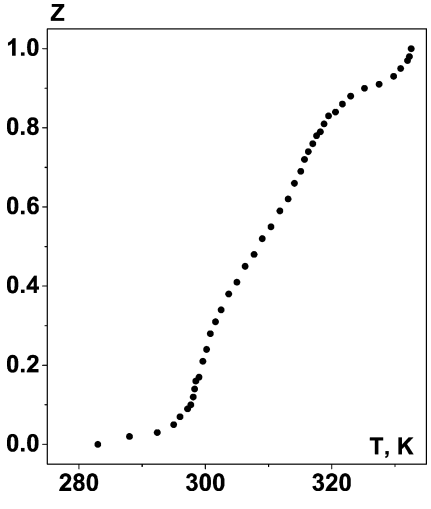

Fig. 6. The vertical temperature profile with gradient 118 K/m, in the core of a turbulent flow at grids oscillation frequency f=10.5 Hz. Here Z is the normalized vertical coordinate, measured in units of Z_{max}=290 mm

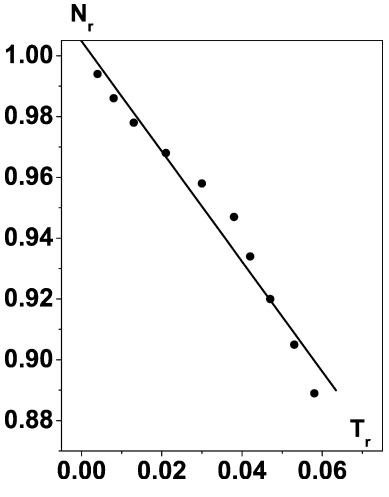

Fig. 8. Normalized particle number density $N_r \equiv \frac{\bar{N}}{\bar{N}_0}$ versus normalized temperature difference $T_r \equiv \frac{(\bar{T}-\bar{T}_0)}{\bar{T}_0}$ in the turbulent non-isothermal flow

The variation of the obtained vertical distributions between these strips was very small. Therefore, in Fig. 8 we used the spatial average over vertical strips and the ensemble average over 100 images of the vertical distributions of the intensity of the scattered light.

The temperature difference between the top and bottom walls of the chamber in the experiment, corresponding to the data shown in Fig. 8, was the same as in Fig. 6. The normalized local mean temperatures (the relative temperature differences $\frac{\bar{T}-\bar{T}_0}{\bar{T}_0}$) in Fig. 8 correspond to the different points inside the probed region. In particular, the location of the point with the reference temperature $\bar{T}_0$is Z=0.135 (the lowest point of the probed region). Here Z is a dimensionless vertical coordinate measured in the units of the height of the chamber, and Z=0 at the bottom of the chamber. The point with the maximum relative temperature difference is the highest point of the probed region at Z=0.865. We also performed experiments with a different mean temperature gradient (one half of that shown in Fig. 6). The results obtained are not presented in Fig. 8 since they are the same. The size of the probed region does not affect the obtained results.

Note that, for each experiment, before starting measurements we let the system run for some time (up to 30 min after smoke injection into the flow with steady mean temperature gradient) in order to attain a stationary state. The time interval required for the formation of a mean temperature gradient was about one hour.

5 Discussion

In order to explain the observed vertical profiles of the mean number density of particles (the dependence of N_r on T_r as shown in Fig. 8), consider Eqs. 2 and 3. If one does not take into account the term $\bar{N}\mathbf{V}_{\text{eff}}$in Eq. 2 for the mean number density of particles, this equation reads $\frac{\partial \bar{N}}{\partial t} = D_T \Delta \bar{N}$, where we neglected a small mean fluid velocity $\bar{\mathbf{V}}_p$and a small molecular mean flux of particles (that corresponds to the conditions in our experiment). Here D_T is the turbulent diffusion coefficient. The steady-state solution of this equation is $\bar{N} = \text{const}$. However, our measurements demonstrate that the solution $\bar{N} = \text{const}$. is valid only for the isothermal turbulent flow; in other words when $\bar{T} = \text{const}$. Let us take into account the effect of turbulent thermal diffusion by including the term $\bar{N}\mathbf{V}_{\text{eff}}$in Eq. 2. Now the steady-state solution of this equation for the non-inertial particles reads: $\frac{\nabla \bar{N}}{\bar{N}} = -\frac{\nabla \bar{T}}{\bar{T}}$. This yields $\frac{\bar{N}}{\bar{N}_0} = 1 - \frac{(\bar{T}-\bar{T}_0)}{\bar{T}_0}$, where $\bar{T} - \bar{T}_0 \ll \bar{T}_0$. In our experiments with particles of sizes 0.5–2 μm, we found that

$$\frac{\bar{N}}{\bar{N}_0} = 1 - \alpha \frac{\bar{T} - \bar{T}_0}{\bar{T}_0}, \qquad (12)$$

where the coefficient α=1.7 (in other words α>1). The deviation of the coefficient α from 1 can be caused by a small yet finite inertia of the particles and a dependence of the coefficient α on the mean temperature gradient. The exact value of the parameter α for inertial particles cannot be found in the framework of our theory (Elperin et al. 1996a, 1997, 1998a, 2000b, 2001) for the condition of this experiment. However, in all experiments performed for different ranges of parameters, α was more than 1, in agreement with the theory, which predicts α=1 for the non-inertial particles, and α>1 for inertial particles. These experiments were performed for different Reynolds numbers $Re=uL/\nu$ (in the range 150–300). However, the dependence of the parameter α on the Reynolds number in this range is very weak.

Remarkably, the small mean flow velocity in the vertical direction in the isothermal flow is directed downwards, while in the flow with the imposed mean temperature gradient it is directed upwards. Therefore, the weak mean flow can only dampen the observed effect of turbulent thermal diffusion. It is also important to note that the contribution of the mean flow to the spatial distribution of particles is negligibly small. Indeed, the normalized distribution of the scattered light intensity, as measured in the different vertical strips in the flow in the regions where the mean flow velocity and coefficient of turbulent diffusion vary strongly (by an order of magnitude) are practically identical (the difference is about 1%).

In Fig. 9, we showed the normalized average distributions of the intensity of scattered light in isothermal,$E_r(Z)$, and non-isothermal, $E_r^T(Z)$, flows. A significant difference between the scattered light intensity distributions in these two cases can be clearly seen. Scattered light intensity drops from the top to the bottom of the test section more sharply in the isothermal flow than that in the non-isothermal case. The obtained light distributions were approximated by a smooth function for further data processing. Intensity of the incident light in the light sheet decreases from the top of the light sheet (Z=200 mm) to the bottom (Z=0 mm) of the chamber, mainly due to the divergence of the light sheet. This causes a decrease in the intensity of the light scattered by seeding particles from the top to the bottom in the isothermal case (see Fig. 9). The situation changes drastically in the non-isothermal case. Indeed, due to the effect of turbulent thermal diffusion, the seeding particles are accumulated in the vicinity of the minimum of the mean temperature (at the bottom of

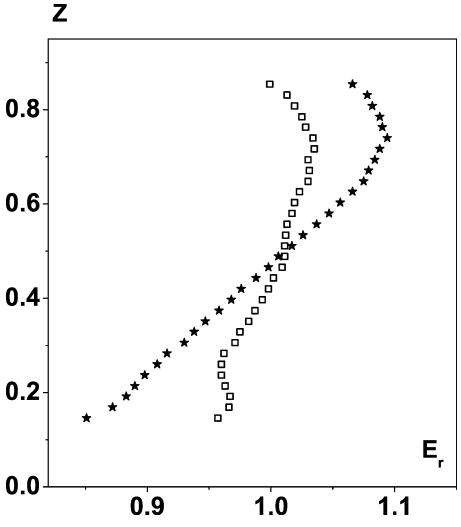

Fig. 9. The normalized average distributions of the intensity of scattered light in isothermal flows E_r(asterisks), and non-isothermal flows E_r^T(squares)

the chamber, Z=0). As a result, the intensity of the scattered light in the non-isothermal case is distributed more uniformly (see Fig. 9) than in the isothermal case. Therefore, the curves presented in Fig. 9 qualitatively confirm the existence of the effect of turbulent thermal diffusion.

The ratio $\frac{E_r^T}{E_r}$of these two curves, as a function of the normalized vertical coordinate Z demonstrates the redistribution of particles in the presence of the mean temperature gradient (see Fig. 10). Finally, let us consider the possible influence of a change in the turbulent diffusion coefficient in the vertical direction, $D_Z^T = u_z L_z$, in the presence of the mean temperature gradient. The measured dependencies of D_Z^Ton the normalized vertical coordinate Z for the isothermal and non-isothermal flows are shown in Fig. 11. Inspection of Fig. 11 shows that the difference in the turbulent diffusion coefficient in both cases is of the order of 10%. As we discussed above (see the discussion of results shown in Fig. 7), this change in the turbulent diffusion coefficient has a negligible effect (less than 0.1%) on the number density distribution of tracer particles. Indeed, as can be seen from Eq. 7, the effective velocity $\mathbf{V}_{\text{eff}} \propto D_T$. Therefore, the turbulent diffusion coefficient does not appear in the stationary solution of Eq. 2; in other words $\bar{N} \propto \exp\left[\int \left(\frac{|\mathbf{V}_{\text{eff}}|}{D_T}\right) dZ\right]$(we neglect very small mean fluid velocities here). The latter conclusion was also confirmed by the measurements performed with the mean temperature gradient reduced by a factor of 2, that yield practically the same results.

The number density of particles in our experiments was of the order of 10^{10} particles per cubic meter. Therefore, the distance between particles is of the order of 1 mm, and their collision rate is negligibly small. Indeed, the calculation of the particle collision rate, using the Saffman-Turner formula (Saffman and Turner 1956), confirmed the latter conclusion. Therefore we did not observe coalescence of particles in our experiments. The effect of the gravitational settling of small particles (0.5–1 μm) is negligibly small as well, since the terminal fall velocity of these particles is less than 0.01 cm/s.

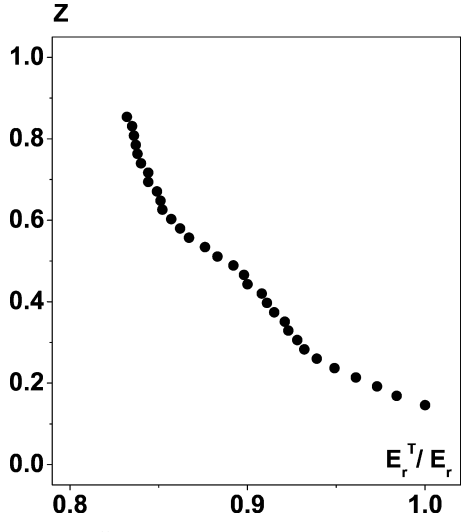

Fig. 10. $\frac{E_r^T}{E_r}$(the ratio of the normalized average distributions of the intensities of scattered light in the non-isothermal and isothermal flows) versus the normalized vertical coordinate Z

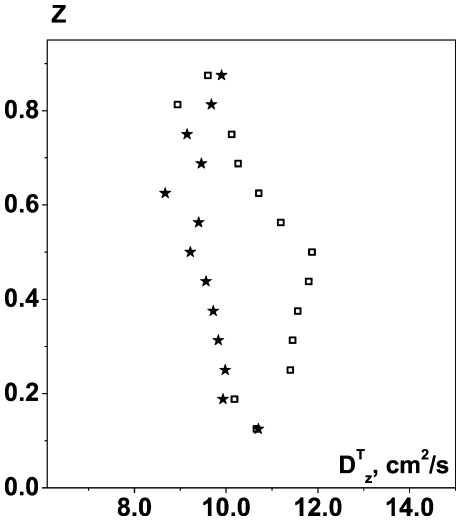

Fig. 11. The measured dependencies of D_z^Tversus the normalized vertical coordinate Z, for isothermal flow (asterisks) and non-isothermal flow (squares)

Due to the effect of turbulent thermal diffusion, particles are redistributed in the vertical direction in the chamber. Particles are accumulated in regions with minimum mean temperature (in the lower part of the chamber), and there is outflow of particles from the upper part of the chamber where the mean temperature is higher. The spatial-temporal evolution of the normalized number density of particles N_r is governed by the conservation law of the total number of particles (see Eqs. 2and 3). Some fraction of the particles sticks to the walls of the chamber, and the total number of particles slowly decreases without the injection of new particles. The characteristic time of this decrease is of the order of 15 min. However, the spatial distribution of the normalized number density of particles does not change in time.

The uncertainty in the measurements of the absolute value of the intensity of the scattered light is of the order of 0.8%. The total error in our measurements is determined by $\frac{\left(\frac{\Delta \bar{N}}{\bar{N}} + \frac{\Delta \bar{T}}{\bar{T}}\right)}{\sqrt{Q}} \approx 0.3\%$(see Eq. 12), where $\Delta \bar{T}$=0.1 K is the accuracy of the temperature measurements, $\frac{\Delta \bar{N}}{\bar{N}}$=0.8% is the accuracy of the mean number density measurements, and Q=8 is the number of experiments. The total variation of the normalized particle number density due to the effect of turbulent thermal diffusion is more than 10% (see Fig. 8). Therefore, since the relative accuracy of the measurements is less than 3%, it is high enough to detect this effect. Therefore, our experiments confirmed the existence of the turbulent thermal diffusion effect predicted theoretically by Elperin et al. (1996a, 1997).

References

Becker HA, Hottel HC, Williams GC (1967) On the light-scatter technique for the study of turbulence and mixing. J Fluid Mech 30:259–284

Bohren CF, Huffman DR (1983) Absorption and scattering of light by small particles. Wiley, New York

Chapman S (1917) On the kinetic theory of a gas: Part II. A composite monatomic gas, diffusion, viscosity and thermal conduction. Phil T Roy Soc A 217:118–192
Chapman S, Dootson FW (1917) A note on thermal diffusion. Philos Mag 33:248–253
De Silva IPD, Fernando HJS (1994) Oscillating grids as a source of nearly isotropic turbulence. Phys Fluids 6:2455–2464
Eaton JK, Fessler JR (1994) Preferential concentration of particles by turbulence. Int J Multiphas Flow 20:169–209
Eidelman A, Elperin T, Kapusta A, Kleeorin N, Krein A, Rogachevskii I (2002) Oscillating grids turbulence generator for turbulent transport studies. Nonlinear Proc Geoph 9:201–205
Elperin T, Kleeorin N, Rogachevskii I (1996a) Turbulent thermal diffision of small inertial particles. Phys Rev Lett 76:224–228
Elperin T, Kleeorin N, Rogachevskii I (1996b) Self-excitation of fluctuations of inertial particles concentration in turbulent fluid flow. Phys Rev Lett 77:5373–5376
Elperin T, Kleeorin N, Rogachevskii I (1997) Turbulent barodiffusion, turbulent thermal diffusion and large-scale instability in gases. Phys Rev E 55:2713–2721
Elperin T, Kleeorin N, Rogachevskii I (1998a) Formation of inhomogeneities in two-phase low-mach-number compressible turbulent flows. Int J Multiphas Flow 24:1163–1182
Elperin T, Kleeorin N, Rogachevskii I (1998b) Anomalous scalings for fluctuations of inertial particles concentration and large-scale dynamics. Phys Rev E 58:3113–3124
Elperin T, Kleeorin N, Rogachevskii I (2000a) Mechanisms of formation of aerosol and gaseous inhomogeneities in the turbulent atmosphere. Atmos Res 53:117–129
Elperin T, Kleeorin N, Rogachevskii I, Sokoloff D (2000b) Passive scalar transport in a random flow with a finite renewal time: mean-field equations. Phys Rev E 61:2617–2625
Elperin T, Kleeorin N, Rogachevskii I, Sokoloff D (2000c) Turbulent transport of atmospheric aerosols and formation of large-scale structures. Phys Chem Earth A 25:797–803
Elperin T, Kleeorin N, Rogachevskii I, Sokoloff D (2001) Mean-field theory for a passive scalar advected by a turbulent velocity field with a random renewal time. Phys Rev E 64:026304(1–9)
Elperin T, Kleeorin N, L'vov V, Rogachevskii I, Sokoloff D (2002) The clustering instability of inertial particles spatial distribution in turbulent flows. Phys Rev E 66:036302(1–16)
Enskog D (1911) Bemerkungen zu einer fundamentalgleichung in der kinetischen gastheorie. Physik Z 12:533–539
Guibert P, Durget M, Murat M (2001) Concentration fields in a confined two-gas mixture and engine in cylinder flow: laser tomography measurements by Mie scattering. Exp Fluids 31: 630–642
Hopfinger EJ, Toly J-A (1976) Spatially decaying turbulence and its relation to mixing across density interfaces. J Fluid Mech 78:155–175
Kit E, Strang EJ, Fernando HJS (1997) Measurement of turbulence near shear-free density interfaces. J Fluid Mech 334:293–314
Maxey MR (1987) The gravitational settling of aerosol particles in homogeneous turbulence and random flow field. J Fluid Mech 174:441–465
McComb WD (1990) The physics of fluid turbulence. Clarendon, Oxford, UK
Pandya RVR, Mashayek F (2002) Turbulent thermal diffusion and barodiffusion of passive scalar and dispersed phase of particles in turbulent flows. Phys Rev Lett 88:044501 (1–4)
Raffel M, Willert C, Kompenhans J (1998) Particle Image Velocimetry. Springer, Berlin Heidelberg New York
Saffman PG, Turner JS (1956) On the collision of drops in turbulent clouds. J Fluid Mech 1:16–30
Sandham ND (2001) A review of progress on direct and large eddy simulation. ERCOFTAC Bull 48:7–9
Shy SS, Tang CY, Fann SY (1997) A nearly isotropic turbulence generated by a pair of vibrating grids. Exp Therm Fluid Sci 14:251–262
Srdic A, Fernando HJS, Montenegro L (1996) Generation of nearly isotropic turbulence using two oscillating grids. Exp Fluids 20:395–397
Stock D (1996) Particle dispersion in flowing gases. ASME J Fluid Eng 118:4-17
Taylor GI (1921) Diffusion by continuous movements. P Lond Math Soc 20:196–212
Thompson SM, Turner JS (1975) Mixing across an interface due to turbulence generated by an oscillating grid. J Fluid Mech 67:349–368
Tyndall J (1870) On dust and disease. P Roy Inst GB 6:1–14